Kobe University Repository : Kernel

PDF issue: 2025-12-05

Solution-processed silicon quantum dot photocathode for hydrogen evolution

Takada, Miho
Inoue, Kosuke
Sugimoto, Hiroshi
Fujii, Minoru

(Citation)
Nanotechnology,32(48):485709

(Issue Date)
2021-11-26

(Resource Type)
journal article

(Version)
Accepted Manuscript

(Rights)
© 2021 IOP Publishing Ltd. This is the Accepted Manuscript version of an article accepted for publication in Nanotechnology. IOP Publishing Ltd is not responsible for any errors or omissions in this version of the manuscript or any version derived from it. The Version of Record is available online at https://doi.org/10.1088/1361-…

(URL)
https://hdl.handle.net/20.500.14094/90009371

Solution- Processed Silicon Quantum Dot Photocathode for Hydrogen Evolution

Miho Takada, Kosuke Inoue, Hiroshi Sugimoto* and Minoru Fujii*

Department of Electrical and Electronic Engineering, Graduate school of Engineering, Kobe University, Rokkodai, Nada, Kobe 657-8501, Japan

E-mail: fujii@eedept.kobe-u.ac.jp

Received xxxxxx
Accepted for publication xxxxxx
Published xxxxxx

Abstract

The photoelectrochemical response of a photocathode made from a colloidal solution of boron (B) and phosphorus (P) codoped silicon (Si) quantum dots (QDs) 2 to 11 nm in diameters is studied. Since codoped Si QDs are dispersible in alcohol and water due to the hydrophilic surface, a photoelectrode with smooth surface is produced by drop-coating the QD solution on an indium tin oxide (ITO) substrate. The codoping provides high oxidation resistance to Si QDs and makes the electrode operate as a photocathode. The photoelectrochemical response of a Si QD photoelectrode depends strongly on the size of QDs; there is a transition from anodic to cathodic photocurrent around 4 nm in diameter. Below the size, anodic photocurrent due to self-oxidation of Si QDs is observed, while above the size, cathodic photocurrent due to electron transfer across the interface is observed. The cathodic photocurrent increases with increasing the size, and in some samples, it is observed for more than 3000 sec under intermittent light irradiation.

Keywords: photocathode, quantum dot, silicon, hydrogen evolution

1. Introduction

A colloidal solution of quantum dots (QDs) can be a precursor to produce QD solids or films by a vacuum-free printing process for flexible light emitting diodes (LEDs) [1], solar cells [2] and thin film transistors [3,4]. It is also a material for the production of QDs photoelectrodes for hydrogen evolution [5–8] and carbon dioxide reduction [9,10]. A QD-based photoelectrode has several superior properties such as the large freedom to control the band gap energy, the large surface-to-volume ratio, and the very small migration distance for photogenerated carriers to reach the surface [11–13]. Zhao *et al*. demonstrated that quantum size effects play an important role to determine the photocatalytic hydrogen generation rate in cadmium selenide (CdSe) QDs [5]. Shi *et al*. showed that tuning of the energy level structure of cadmium sulfide (CdS) QDs by selenium (Se) doping enhances the hydrogen evolution performance [8]. These cadmium (Cd)-chalcogenide QDs are also used as a sensitizer to enhance the effective absorption cross-section of a photoelectrode made from wide band gap semiconductor [14]. For example, Hongjin *et al*. achieved a Faradaic efficiency of 99.5 % for photoelectrochemical hydrogen production in nickel oxide (NiO) photoelectrodes with different-size CdSe QDs on the surface [15]. So far, almost

 © xxxx IOP Publishing Ltd

all researches on QDs-based photoelectrodes are utilizing Cd-chalcogenide QDs due mainly to the availability of the high-quality colloidal solution. However, the toxicity of Cd is always concern for the further development.

In contrast to Cd-chalcogenides, silicon (Si) is an environmentally friendly semiconductor material. The band gap is in the near infrared range (1.12 eV) and the conduction band edge is much higher than the proton reduction potential [16–18]. Therefore, it is a potentially suitable material for a photocathode for hydrogen evolution. Several types of nanoscale Si crystals, such as porous Si [19–21] and Si nanowires [12,22–24], have been developed as a material for a photocathode. These Si nanostructures are produced by electrochemical etching, metal-assisted etching, chemical vapor deposition, etc. On the other hand, production of a photoelectrode from a colloidal solution of Si QDs by a solution-based process is very rare. Although a solution of porous Si nanoparticles, which are agglomerates of Si nanocrystals, was used to produce a photocathode by a drop-casting process [21], the complicated structure hinders detailed analyses of the size dependence of the photoelectrochemical property.

In applications of Si QDs for a photocathode, the largest concern is the surface oxidation; formation of a kinetic barrier degrades the performance of the photoelectrode. Recently, we have developed Si QDs having much higher oxidation resistance than conventional Si QDs. The Si QDs have a heavily boron (B) and phosphorous (P) codoped amorphous shell [25,26] as confirmed by atom probe tomography and transmission electron microscopy (TEM) [27–29]. The shell induces characteristic surface properties to Si QDs such as the negative surface potential (ζ potential: ~-30 meV) [30], the high dispersibility in water without organic ligands [31], and the high oxidation resistance [32]. B atoms accumulated on the surface are considered to be responsible for these properties [33]. To the ligand-free bare surface of a B and P codoped Si QD, molecules in a solution can easily access, and thus efficient charge transfer reaction is expected. In fact, chemical doping [34] and various photocatalytic reactions [36], including photocatalytic hydrogen evolution [32], have been observed.

This work is an extension of the previous work on photocatalytic hydrogen evolution by B and P codoped Si QDs [32]. In this work, we fabricate a photoelectrode from colloidal solutions of codoped Si QDs with the diameters in the range 2 to 11 nm, and study the photoelectrochemical properties. We show that B and P codoping modifies the photoelectrochemical response of Si QDs significantly. In a photoelectrode produced from undoped Si QDs, the photoresponse is often not observed or sometimes anodic photocurrent is observed. The anodic photocurrent indicates that photoexcited holes are consumed by self-oxidation, and photoexcited electrons are transferred to the back-contact. On the other hand, in codoped Si QDs, cathodic photocurrent is observed when the size is relatively large. Therefore, in codoped Si QDs, photoexcited holes are transferred to the back-contact before self-oxidation of Si QDs proceeds, and photoexcited electrons reduce protons. We also show that the cathodic photocurrent increases with increasing the size of codoped Si QDs. The present results indicate that high oxidation resistance achieved by B and P codoping largely improves photoelectrochemical responses of Si QD photocathodes.

2. Experimental section

Colloidal solutions of B and P codoped Si QDs were fabricated by a cosputtering method. Details of the preparation procedure are shown in our previous papers [25,26]. Si, silicon dioxide (SiO_2), boron trioxide (B_2O_3), and phosphorus pentoxide (P_2O_5) were simultaneously sputtered, and a Si-rich borophosphosilicate glass (BPSG) film was deposited on a stainless-steel plate. The film was peeled off from the plate and annealed in a N_2 gas atmosphere at 1000-1250 °C for 30 min to grow codoped Si QDs in a BPSG matrix. The size of the Si QDs depends on the annealing temperature. Our previous TEM studies revealed that in this temperature range, the average diameter of Si QDs changes from 2-11 nm [30,32]. Si QDs were extracted from a BPSG matrix by hydrofluoric acid (HF) etching and dispersed in methanol. As references, undoped Si QDs were also produced by a similar method, i.e., Si and SiO_2 were sputter-deposited simultaneously and annealed at 1000-1200 °C. Since undoped Si QDs form agglomerates after HF etching, the size cannot be determined precisely. Before HF etching, i.e., in a silica matrix, the average diameter of undoped Si QDs changes from 4.2 nm to 5.4 nm in the annealing temperature range of 1150-1200 °C [36].

Figure 1a shows a photograph of a water solution of codoped Si QDs (5.9 nm in average diameter). The solution is clear and light scattering by agglomerates is not observed. The high dispersibility of codoped Si QDs in water is due to the negative surface potential induced by doping [31]. Note that in the case of undoped Si QDs prepared by a similar process, large agglomerates precipitate immediately. Figure 1b and c shows TEM (JEM-2010, JEOL) images of codoped Si QDs grown at 1150 and 1200 °C. The high resolution images are shown in the insets. For the TEM observations, a methanol solution of Si QDs was dropped on a carbon-coated copper mesh. Lattice fringes corresponding to {111} planes of Si crystal can be seen. The average diameters (d_{ave}) and the standard deviations (σ) obtained from TEM observations are d_{ave} = 5.9 nm (σ = 1.2 nm) and d_{ave} = 8.6 nm (σ = 2.0 nm) for codoped Si QDs grown at 1150 and 1200 °C, respectively.

Figure 1d shows PL spectra of Si QDs in water excited at 405 nm. The average diameter is changed from 2.0 to 8.6 nm.

A high-energy shift of the PL peak with decreasing the size is clearly observed [30]. We have studied the size dependence of the PL energy in detail in previous work and found that the PL peak energy of codoped Si QDs is several hundred meV lower in energy than that of undoped Si QDs with comparable sizes [37]. The low-energy shift by B and P codoping indicates that the PL arises from donor-to-acceptor states transitions. The formation of donor and acceptor states was proved by scanning tunneling spectroscopy (STS) [38]. The PL bands in Figure 1d are very broad. This is partly due to the size distribution [39]. However, even without size distribution, i.e., in single dot spectroscopy, the PL bands of B and P codoped Si QDs are very broad, i.e., ~250 mV or even more at room temperature [39]. Codoped Si QDs are slightly p-type [40]; p-type operation is reported in MOS FETs produced from codoped Si QDs 6.9 nm in average diameter [41].

Figure 1e shows the process to produce a Si QD photoelectrode. A methanol solution (~6 µL) of Si QDs (10 µg) was dropped onto an indium tin oxide (ITO) film (150 nm in thickness) on a glass plate (15 mm×5 mm) after the UV-ozone cleaning. The electrode was then annealed in vacuum (5×10^{-5} Torr) at 250 °C for 30 min to remove solvents. Finally, the area to have contact with a solvent (7.5 mm× 5 mm) was defined by covering the peripheral region by epoxy resin.

Photoelectrochemical measurements were carried out using a conventional three-electrode setup (SP-300, BioLogic) shown in Figure 1e by using a Pt coil as a counter electrode and an Ag/AgCl electrode as a reference electrode. A 0.5 M Na_2SO_4 solution was used as the electrolyte. Prior to measurements, a solution was purged by Ar gas to remove dissolved oxygen. A diode laser (405 nm, 100 mW) was used as a light source. Linear sweep voltammetry (LSV) was performed in a 0.15 to -0.45 V vs RHE range. The scan rate was 20 mV s^{-1}. In the Supporting Information (Figure S1), the relation between the electrode potential and the highest occupied molecular orbital (HOMO) and (lowest unoccupied molecular orbital (LUMO) levels of Si QDs are shown [40]. The photocurrent response under the intermittent light irradiation was measured at constant applied potential of -0.25 V vs RHE. We confirmed that no photoresponse is observed without Si QDs, i.e., in a bare ITO electrode (Figure S2 in the Supporting Information).

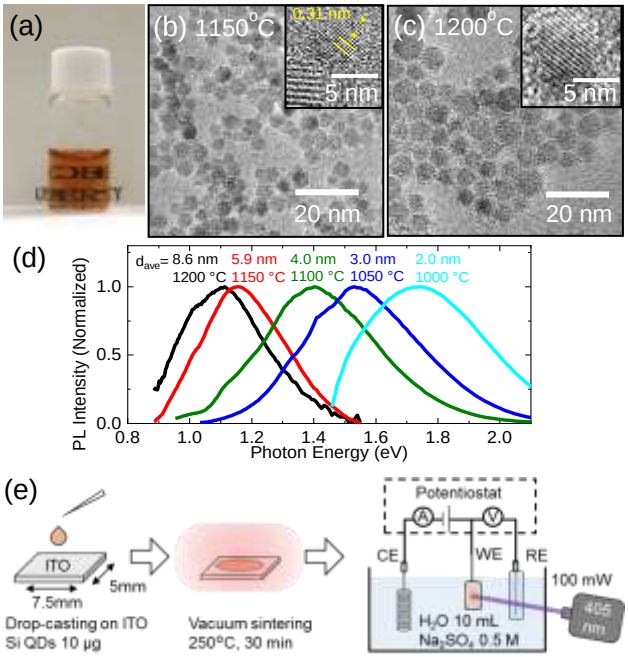

Figure 1. (a) Photograph of a water solution of codoped Si QDs. (b,c) TEM images of Si QDs grown at (b) 1150, and (c) 1200 °C. The average diameters estimated from TEM images are 5.9 and 8.6 nm, respectively. (d) PL spectra of water solutions of Si QDs with different diameters. The average diameters and growth temperatures are shown in the figure. (e) Fabrication of Si QDs photoelectrode and schematic of three electrodes setup. A Pt coil counter electrode and an Ag/AgCl reference electrode were immersed in water containing 0.5 M Na_2SO_4 as a supporting electrolyte.

3. Results and discussion

Figure 2a shows a photo of a photoelectrode produced from a water solution of B and P codoped Si QDs 8.6 nm in diameter. Since Si QDs are well-dispersed in a solution, a flat film is formed by drop-coating. In the Supporting Information (Figure S4), photos of Si QDs photoelectrodes produced from other size codoped Si QDs are shown. The films are very stable and the morphology does not change by photoelectrochemical experiments described below (Figure S3 in the Supporting Information). Figure 2b shows a cross-sectional scanning electron microscope (SEM) (JSM-7100F, JEOL) image of a Si QDs photoelectrode. The image was taken after modulated light irradiation for 3000 sec under constant bias (-0.25 V vs RHE). The average diameter of Si QDs is 5.9 nm. A dense film of Si QDs is formed. The thickness of the Si QD layer is ~340 nm. This indicates that about 60 layers of Si QDs are formed. Figure 2c shows an atomic force microscope (AFM) (TT-2 AFM, AFM workshop) image. The root mean square roughness is 5.0 nm,

which is comparable to the QD size. It should be stressed here that a uniform film like Figure 2a cannot be produced from undoped Si QDs because of the agglomeration in water (see photos of electrodes produced from undoped Si QDs in the Supporting Information (Figure S5)).

Figure 2d shows a Raman spectrum of a Si QDs photoelectrode produced from Si QDs 5.9 nm in diameter (excitation: 488.0 nm, 1 mW) (solid line). A TO phonon mode of Si crystal at 520 cm^{-1} is clearly seen, indicating the high crystallinity of the Si QDs. A broad background below 500 cm^{-1} comes from an ITO/glass substrate (dotted line) and a heavily B and P doped amorphous shell of a Si QD [42]. The broad band around 650 cm^{-1} also arises from a heavily B and P codoped amorphous shell [42].

Figure 2e shows the light transmittance spectra of electrodes produced from Si QDs 2.0, 5.9, and 8.6 nm in average diameters. The transmission loss at the long wavelength side is mainly due to scattering and reflection, while that at the short wavelength side is due to absorption by Si QDs. With decreasing the size of Si QDs, the absorption becomes small even though the amount (weight) of Si QDs are fixed. This is due to the high-energy shift of the band gap by the quantum size effect. The decrease of the absorption with decreasing the size can also be seen in the color of the electrodes (Figure S4 in the Supporting Information).

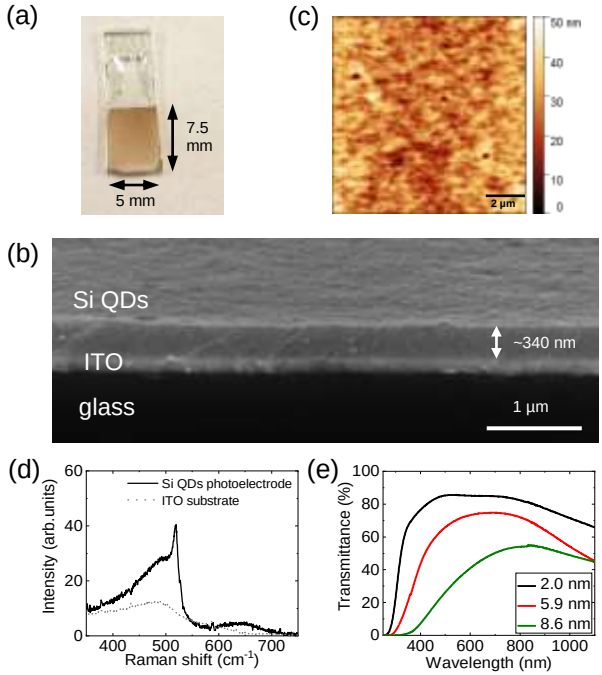

Figure 2. (a) Photograph of a photoelectrode of Si QDs 8.6 nm in diameter. (b) Cross-sectional SEM image (10° tilted), (c) AFM image, and (d) Raman scattering spectrum of a photoelectrode of Si QDs 5.9 nm in diameter. In (d), a spectrum of an ITO substrate is also shown (dot line). (e) Light transmittance spectra of Si QDs photoelectrodes with different particle diameters.

First, we study photoelectrochemical properties of a photoelectrode produced from undoped Si QDs. Since undoped Si QDs are not dispersible in water and form agglomerates, the electrode is not uniform (Figure S5 in the Supporting Information). Although the morphology is not nice, we can still measure the LSV. Figure 3a shows one of the results. The sweep range is 0.15 to -0.45 V vs RHE. The shaded and unshaded regions correspond to dark and light irradiation, respectively. Under light irradiation, anodic current is observed. A possible mechanism of the anodic photocurrent is that a photoexcited electron is transferred to the back-contact and a hole is consumed by self-oxidation of a Si QD by the following reaction [43],

$$Si + 4h^+ + 2H_2O \rightarrow SiO_2 + 4H^+ , \quad (1)$$

where h^+ is a photoexcited hole in a Si QD. Therefore, photoexcited electrons do not reduce protons in undoped Si QDs. It should be noted here that the anodic photocurrent similar to Figure 3a was observed for a few undoped Si QDs samples, but in some samples, photoresponses were not observed (Figure S6 in the Supporting Information). Furthermore, no clear size dependence was observed in the photoresponse of undoped Si QDs. This result suggests that previously observed H_2 generation by undoped Si QDs under light irradiation [32] is at least partly due to the self-oxidation.

Figure 3b-d shows the linear sweep voltammograms of photoelectrodes produced from codoped Si QDs 2.0, 5.9 and 8.6 nm in average diameters, respectively. Different photoresponses are observed for different size Si QDs. Furthermore, the level of the background current is different. However, since no systematic trends were observed for the background current, in the following, we focus on the photocurrent, i.e., difference of the current between under light irradiation and in dark. In codoped Si QDs 2.0 nm in diameter (Figure 3b), anodic photocurrent similar to that of undoped Si QDs in Figure 3a is observed. On the other hand, in Si QDs 5.9 and 8.6 nm in diameters (Figure 3c and d, respectively), cathodic current is observed under light irradiation. This suggests that photoexcited electrons reduce proton at the surface, and holes are transferred to the back-electrode and oxidize water at the counter electrode.

In Figure 3e, photocurrent under constant bias (-0.10 and -0.20 V vs RHE) is shown as a function of the diameter of codoped Si QDs. We can see clear size dependence; the cathodic photocurrent increases with increasing the size. We can also see a transition from anodic to cathodic photocurrent around 4 nm in diameter. One of the reasons for the photocurrent increase with increasing the size is due to the increase of the light absorption (Figure 2e). However, it cannot explain the transition from anodic to cathodic photocurrent. The observed size dependence suggests that there is competition between anodic photocurrent due to self-

oxidation of Si QDs and cathodic current due to proton reduction. The former is dominant in small codoped Si QDs and undoped Si QDs, while the latter is dominant in large codoped Si QDs. The observation of the cathodic current suggests that self-oxidation in eq. (1) is largely suppressed in relatively large codoped Si QDs.

It is noted that both the photocatalytic proton reduction and the photooxidation of Si QDs results in H_2 generation. In our previous work on H_2 evolution by codoped Si QDs, we studied the amount of H_2 molecules generated in Si QDs-dispersed water under light irradiation [32]. However, in the experiments, the two mechanisms were not clearly distinguished. Combination of the previous results and the present result, i.e., dominance of cathodic photocurrent and suppression of self-oxidation in relatively large codoped Si QDs, suggests that H_2 generation in large codoped Si QDs observed in the previous work is mainly due to photocatalytic proton reduction.

Figure 3f shows the current response under intermittent light irradiation (5 sec on and 5 sec off) under constant bias (-0.25 V vs RHE) for 3000 sec. The average diameter of Si QDs is 5.9 nm. Stable cathodic photocurrent is observed for 3000 sec. However, this is the data of the best sample produced. At the present stage of research, the stability of the cathodic photocurrent depends on samples. Even in electrodes produced from same QD solutions, the stability is different. For example, in the Supporting Information (Figure S7 and S8), the data obtained for different electrodes produced from codoped Si QDs 5.9 and 8.6 nm in diameters, respectively, are shown. In both cases, the stability is different from sample to sample.

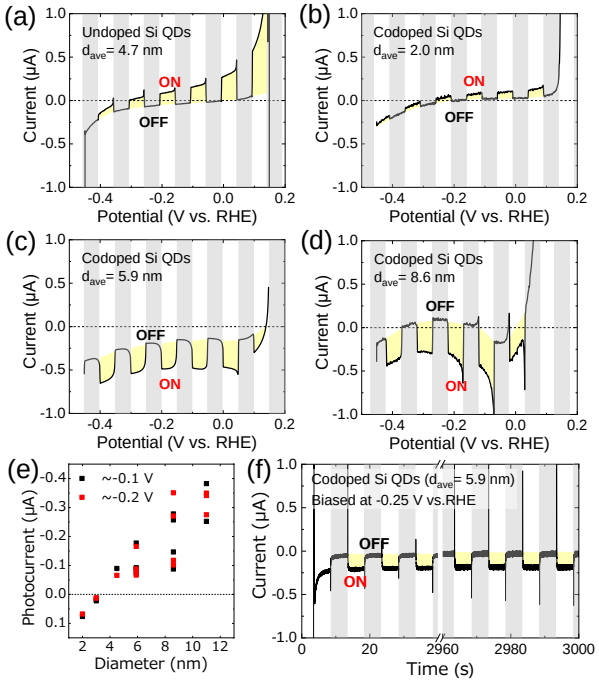

Figure 3. Current response of Si QD photoelectrodes under chopped 405 nm illumination. (a-d) LSVs of (a) undoped and (b-d) codoped Si QDs on ITO substrate. The size of codoped Si QDs is (b) 2.0 nm, (c) 5.9 nm, and (d) 8.6 nm. The scan range is 0.15 to -0.45 V vs RHE, and the scan speed is 20 mV s^{-1}. The shaded and unshaded regions correspond to dark and light irradiation, respectively. (e) Photocurrent of Si QDs photoelectrodes produced from different diameter codoped Si QDs under constant bias (-0.10 and -0.20 V vs RHE). (f) Photocurrent under intermittent light irradiation (5 sec on and 5 sec off) under constant bias (-0.25 V vs RHE) for 3000 sec.

In Figure S9 in the Supporting Information, photoresponses of electrodes produced from codoped Si QDs 5.9 nm in diameter at different pH (3-7) are shown. pH is controlled by adding sulfuric acid. Photocurrent does not strongly depend on pH. Similarly, in Figure S10 in the Supporting Information, photoresponses when different kinds of reducing (sacrificial) agents, i.e., methanol, formaldehyde, ethylenediaminetetraacetic acid (EDTA), sodium sulfite and ascorbic acid, are added are shown. In almost all cases except for the addition of ascorbic acid, the cathodic photocurrent does not change or decreases. The decrease is due to extraction of photoexcited holes by sacrificial agents, and resultant decrease of hole transfer to a back contact. At present, the mechanism of the cathodic photocurrent increase by ascorbic acid is not clear. A possible explanation is that it prevents self-oxidation of Si QDs and keeps them fresh.

Finally, in order to study the composition of the surface and the oxidation resistance of different size codoped Si QDs, we perform the X-ray photoelectron spectroscopy (XPS) (PHI X-tool, ULVAC-PHI) before and after the intermittent (5 sec on and 5 sec off) light irradiation for 3000 sec under a constant bias (-0.25 V vs RHE) in water. Figure 4a-c shows XPS spectra of Si 2p, P 2p and B 1s core electrons, respectively. The black and red curves are the data obtained before and after light irradiation, respectively. Before irradiation, in Si QDs 2.0 nm in diameter, the signals from oxidation states of Si (Si^{2+} or Si^{3+}) dominate the spectrum, while in Si QDs 5.9 and 8.6 nm in diameters, the Si^{0+} signal is dominant. This means that already during storage of Si QDs in methanol and water, oxidation proceeds in small Si QDs. In 2.0 nm diameter Si QDs, P 2p and B 1s signals are much weaker than those of 5.9 and 8.6 nm diameter Si QDs. In particular, P 2p signal is barely observed. This indicates that the B and P codoped shell is much thinner in 2.0 nm diameter Si QDs than in larger Si QDs. In other words, the surface structure of 2.0 nm diameter Si QDs is similar to that of undoped Si QDs, and thus they exhibit similar photoelectrochemical responses.

After light irradiation, the XPS spectra slightly change. In Si QDs 2.0 nm in diameter, the Si^{0+} signal decreases slightly and those of the oxidation states (Si^{2+} or Si^{3+}) increase. This suggests formation of Si-O bonds during light irradiation. Similar change is observed in Si QDs 5.9 nm in diameter. In Si QDs 8.6 nm in diameter, the change of the Si 2p signal is very small, although still exists. In Si QDs 5.9 nm in diameter, both the P 2p and B1s signals become small, while, in Si QDs 8.6 nm in diameter, the signals are almost unaffected.

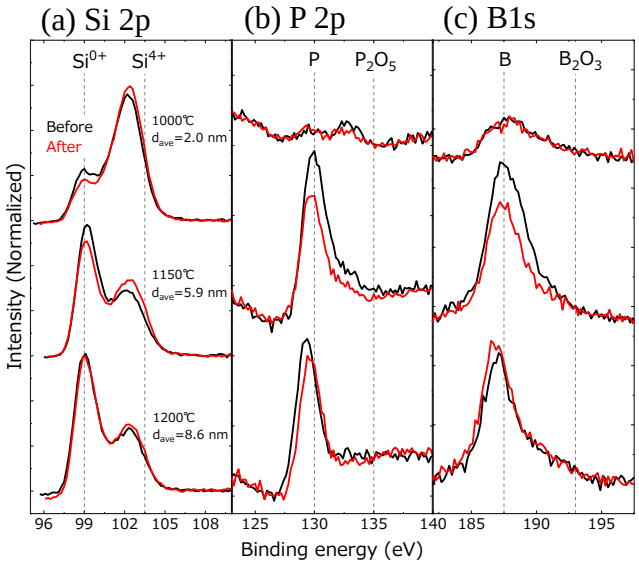

Figure 4. XPS spectra of Si QDs photoelectrodes before (black line) and after (red line) intermittent (5 sec on and 5 sec off) light irradiation for 3000 sec under constant bias (-0.25 V vs RHE); (a) Si 2p, (b) P 2p, (c) B 1s. The data of Si QDs 2.0, 5.9 and 8.6 nm in diameters are shown.

3. Conclusion

We have developed Si QDs photoelectrodes from colloidal solutions of B and P codoped Si QDs. Since codoped Si QDs are well dispersed in water and does not form agglomerates, smooth QDs films were produced by drop-coating. We found that the photoelectrochemical response depends strongly on the size of Si QDs. When the diameter is smaller than around 4 nm, anodic photocurrent due to self-oxidation of Si QDs was observed, while cathodic photocurrent due to proton reduction was observed for larger Si QDs. In some samples, cathodic photocurrent was observed for more than 3000 sec under the intermittent light irradiation. The present results suggest that B and P codoping significantly improves photoelectrochemical properties of Si QDs photocathodes and thus opens a new route to realize Si-based high performance photoelectrodes.

Acknowledgements

This work was partly supported by JSPS KAKENHI Grant Nos. 18K14092, 18KK0141, and 19K22111.

ORCID iDs

*Minoru Fujii − orcid.org/0000-0003-4869-7399
*Hiroshi Sugimoto − orcid.org/0000-0002-1520-0940

References

[1] Shirasaki Y, Supran G J, Bawendi M G and Bulović V 2013 Emergence of colloidal quantum-dot light-emitting technologies *Nat. Photonics* **7** 13–23

[2] Carey G H, Abdelhady A L, Ning Z, Thon S M, Bakr O M and Sargent E H 2015 Colloidal Quantum Dot Solar Cells *Chem. Rev.* **115** 12732–63

[3] Dolzhnikov D S, Zhang H, Jang J, Son J S, Panthani M G, Shibata T, Chattopadhyay S and Talapin D V. 2015 Composition-matched molecular "solders" for semiconductors *Science* **347** 425–8

[4] Choi J H, Wang H, Oh S J, Paik T, Jo P S, Sung J, Ye X, Zhao T, Diroll B T, Murray C B and Kagan C R 2016 Exploiting the colloidal nanocrystal library to construct electronic devices *Science* **352** 205–8

[5] Zhao J, Holmes M A and Osterloh F E 2013 Quantum Confinement Controls Photocatalysis: A Free Energy Analysis for Photocatalytic Proton Reduction at CdSe Nanocrystals *ACS Nano* **7** 4316–25

[6] Li H, Wen P, Hoxie A, Dun C, Adhikari S, Li Q, Lu C, Itanze D S, Jiang L, Carroll D, Lachgar A, Qiu Y and Geyer S M 2018 Interface Engineering of Colloidal CdSe Quantum Dot Thin Films as Acid-Stable Photocathodes for Solar-Driven Hydrogen Evolution *ACS Appl. Mater. Interfaces* **10** 17129–39

[7] Liu Y, Dai F, Zhao R, Huai X, Han J and Wang L 2019 Aqueous synthesis of core/shell/shell CdSe/CdS/ZnS quantum dots for photocatalytic hydrogen generation *J. Mater. Sci.* **54** 8571–80

[8] Shi J W, Sun D, Zou Y, Ma D, He C, Ji X and Niu C 2019 Trap-level-tunable Se doped CdS quantum dots with excellent hydrogen evolution performance without co-catalyst *Chem. Eng. J.* **364** 11–9

[9] Wang J, Xia T, Wang L, Zheng X, Qi Z, Gao C, Zhu J, Li Z, Xu H and Xiong Y 2018 Enabling Visible-Light-Driven Selective CO 2 Reduction by Doping Quantum Dots: Trapping Electrons and Suppressing H 2 Evolution *Angew. Chemie Int. Ed.* **57** 16447–51

[10] Xu Y F, Yang M Z, Chen B X, Wang X D, Chen H Y, Kuang D Bin and Su C Y 2017 A CsPbBr3 Perovskite Quantum Dot/Graphene Oxide Composite for Photocatalytic CO2 Reduction *J. Am. Chem. Soc.* **139** 5660–3

[11] Yoon H P, Yuwen Y A, Kendrick C E, Barber G D, Podraza N J, Redwing J M, Mallouk T E, Wronski C R and Mayer T S 2010 Enhanced conversion efficiencies for pillar array solar cells fabricated from crystalline silicon with short minority carrier diffusion lengths *Appl. Phys. Lett.* **96** 213503

[12] Dai P, Xie J, Mayer M T, Yang X, Zhan J and Wang D 2013 Solar Hydrogen Generation by Silicon Nanowires Modified with Platinum Nanoparticle Catalysts by Atomic Layer Deposition *Angew. Chemie Int. Ed.* **52** 11119–23

[13] Osterloh F E 2013 Inorganic nanostructures for photoelectrochemical and photocatalytic water splitting *Chem. Soc. Rev.* **42** 2294–320

[14] Wu H-L, Li X-B, Tung C-H and Wu L-Z 2018 Recent Advances in Sensitized Photocathodes: From Molecular Dyes to Semiconducting Quantum Dots *Adv. Sci.* **5** 1700684

[15] Lv H, Wang C, Li G, Burke R, Krauss T D, Gao Y and Eisenberg R 2017 Semiconductor quantum dot-sensitized rainbow photocathode for effective photoelectrochemical hydrogen generation *Proc. Natl. Acad. Sci. U. S. A.* **114** 11297–302

[16] Fan R, Mi Z and Shen M 2019 Silicon based photoelectrodes for photoelectrochemical water splitting *Opt. Express* **27** A51

[17] Sun K, Shen S, Liang Y, Burrows P E, Mao S S and Wang D 2014 Enabling silicon for Solar-Fuel production *Chem. Rev.* **114** 8662–719

[18] Zhang D, Shi J, Zi W, Wang P and Liu S F 2017 Recent Advances in Photoelectrochemical Applications of Silicon Materials for Solar-to-Chemicals Conversion *ChemSusChem* **10** 4324–41

[19] Zhao Y, Anderson N C, Zhu K, Aguiar J A, Seabold J A, Lagemaat J van de, Branz H M, Neale N R and Oh J 2015 Oxidatively Stable Nanoporous Silicon Photocathodes with Enhanced Onset Voltage for Photoelectrochemical Proton Reduction *Nano Lett.* **15** 2517–25

[20] Chandrasekaran S, Macdonald T J, Mange Y J, Voelcker N H and Nann T 2014 A quantum dot sensitized catalytic porous silicon photocathode *J. Mater. Chem. A* **2** 9478–81

[21] Chandrasekaran S, McInnes S J P, Macdonald T J, Nann T and Voelcker N H 2015 Porous silicon nanoparticles as a nanophotocathode for photoelectrochemical water splitting *RSC Adv.* **5** 85978–82

[22] Oh I, Kye J and Hwang S 2012 Enhanced photoelectrochemical hydrogen production from silicon nanowire array photocathode *Nano Lett.* **12** 298–302

[23] Dasgupta N P, Liu C, Andrews S, Prinz F B and Yang P 2013 Atomic Layer Deposition of Platinum Catalysts on Nanowire Surfaces for Photoelectrochemical Water Reduction *J. Am. Chem. Soc.* **135** 12932–5

[24] Li X, Xiao Y, Zhou K, Wang J, Schweizer S L, Sprafke A, Lee J-H and Wehrspohn R B 2015 Photoelectrochemical hydrogen evolution of tapered silicon nanowires † *Phys. Chem. Chem. Phys* **800** 28–54

[25] Fujii M, Sugimoto H and Imakita K 2016 All-inorganic colloidal silicon nanocrystals - Surface modification by boron and phosphorus co-doping *Nanotechnology* **27** 262001

[26] Fujii M, Sugimoto H and Kano S 2018 Silicon quantum dots with heavily boron and phosphorus codoped shell *Chem. Commun.* **54** 4375

[27] Nomoto K, Sugimoto H, Breen A, Ceguerra A V, Kanno T, Ringer S P, Wurfl I P, Conibeer G and Fujii M 2016 Atom Probe Tomography Analysis of Boron and/or Phosphorus Distribution in Doped Silicon Nanocrystals *J. Phys. Chem. C* **120** 17845–52

[28] Nomoto K, Sugimoto H, Cui X-Y, Ceguerra A V, Fujii M and Ringer S P 2019 Distribution of boron and phosphorus and roles of co-doping in colloidal silicon nanocrystals *Acta Mater.* **178** 186–93

[29] Sugimoto H, Yamamura M, Sakiyama M and Fujii M 2018 Visualizing a core–shell structure of heavily doped silicon quantum dots by electron microscopy using an atomically thin support film *Nanoscale* **10** 7357–62

[30] Sugimoto H, Fujii M, Imakita K, Hayashi S and Akamatsu K 2013 Codoping n- and p-Type Impurities in Colloidal Silicon Nanocrystals: Controlling Luminescence Energy from below Bulk Band Gap to Visible Range *J. Phys. Chem. C* **117** 11850–7

[31] Sugimoto H, Fujii M, Imakita K, Hayashi S and Akamatsu K 2012 All-inorganic near-infrared luminescent colloidal silicon nanocrystals: High dispersibility in polar liquid by phosphorus and boron codoping *J. Phys. Chem. C* **116** 17969–74

[32] Sugimoto H, Zhou H, Takada M, Fushimi J and Fujii M 2020 Visible-light driven photocatalytic hydrogen generation by water-soluble all-inorganic core–shell silicon quantum dots *J. Mater. Chem. A* **8** 15789–94

[33] Wheeler L M, Kramer N J and Kortshagen U R 2018 Thermodynamic Driving Force in the Spontaneous Formation of Inorganic Nanoparticle Solutions *Nano Lett.* **18** 1888–95

[34] Sugimoto H, Hori Y, Imura Y and Fujii M 2017 Charge-Transfer-Induced Photoluminescence Enhancement in Colloidal Silicon Quantum Dots *J. Phys. Chem. C* 121–11962

[35] Kojima T, Sugimoto H and Fujii M 2018 Size-Dependent Photocatalytic Activity of Colloidal Silicon Quantum Dot *J. Phys. Chem. C* **122** 1874–80

[36] Takeoka S, Fujii M and Hayashi S 2000 Size-dependent photoluminescence from surface-oxidized Si nanocrystals in a weak confinement regime *Phys. Rev. B - Condens. Matter Mater. Phys.* **62** 16820–5

[37] Sugimoto H, Yamamura M, Fujii R and Fujii M 2018 Donor-Acceptor Pair Recombination in Size-Purified Silicon Quantum Dots *Nano Lett.* **18** 7282–8

[38] Ashkenazi O, Azulay D, Balberg I, Kano S, Sugimoto H, Fujii M and Millo O 2017 Size-dependent donor and acceptor states in codoped Si nanocrystals studied by scanning tunneling spectroscopy † *Nanoscale* **9**

[39] Kanno T, Sugimoto H, Fucikova A, Valenta J and Fujii M 2016 Single-dot spectroscopy of boron and phosphorus codoped silicon quantum dots *J. Appl. Phys.* **120** 164307

[40] Hori Y, Kano S, Sugimoto H, Imakita K and Fujii M 2016 Size-Dependence of Acceptor and Donor Levels of Boron and Phosphorus Codoped Colloidal Silicon Nanocrystals *Nano Lett.* **16** 2615–20

[41] Kano S, Tada Y, Matsuda S and Fujii M 2018 Solution Processing of Hydrogen-Terminated Silicon Nanocrystal for Flexible Electronic Device *ACS Appl. Mater. Interfaces* **10** 20672–8

[42] Fujii M, Sugimoto H, Hasegawa M and Imakita K 2014 Silicon nanocrystals with high boron and phosphorus concentration hydrophilic shell - Raman scattering and X-ray photoelectron spectroscopic studies *J. Appl. Phys.* **115** 084301

[43] Chen S and Wang L-W 2012 Thermodynamic Oxidation and Reduction Potentials of Photocatalytic Semiconductors in Aqueous Solution *Chem. Mater.* **24** 3659–66